Trailer Electrification – A HIL Approach for MPC Powertrain Control to Ensure Driver Safety in Micromobility

2023-24-0180

Published: August 28, 2023

Marius Miller[1], Markus Pfeil[1], and Ralph Kennel[2]

[1]Ravensburg-Weingarten University

[2]Technical University of Munich

Citation: Miller, M., Pfeil, M., and Kennel, R., "Trailer Electrification – A HIL Approach for MPC Powertrain Control to Ensure Driver Safety in Micromobility," SAE Technical Paper 2023-24-0180, 2023

DOI: https://doi.org/10.4271/2023-24-0180

Received: 13 May 2023 Revised: 29 Jun 2023 Accepted: 30 Jun 2023

Abstract

Bicycle-drawn cargo trailers with an electric drive to enable the transportation of high cargo loads are used as part of the last-mile logistics. Depending on the load, the total mass of a trailer can vary between approx. 50 and 250 kg, potentially more than the mass of the towing bicycle. This can result in major changes in acceleration and braking behavior of the overall system. While existing systems are designed primarily to provide sufficient power, improvements are needed in the powertrain control system in terms of driver safety and comfort. Hence, we propose a novel prototype that allows measurement of the tensile force in the drawbar which can subsequently be used to design a superior control system. In this context, a sinusoidal force input from the cyclist to the trailer according to the cadence of the cyclist is observed. The novelty of this research is to analyze whether torque impulses of the cyclist can be reduced with the help of Model Predictive Control (MPC). In addition, the powertrain of the trailer is intended to support the braking process of the system with regenerative braking. In the context of this research, a first MPC controller design is carried out and analyzed with the help of a Hardware-in-the-Loop (HIL) approach where the microcontroller of the power electronics is included as hardware to ensure the vehicle dynamics control interacts properly with the lower-level field-oriented control. The battery and motor subsystems are simulated in a Typhoon HIL 604, which is supplemented by a vehicle dynamics model of the trailer that is integrated as a Functional Mock-Up Unit (FMU). First results indicate that the MPC longitudinal dynamics controller supports the driver during acceleration, attenuates the sinusoidal oscillations and reduces the force with which the trailer pushes the bicycle during braking.

Introduction

In the course of the debate about a more sustainable mobility, there is also a need to rethink sustainable concepts of delivery traffic. Within the context of distribution logistics, micromobility, which includes small and electrified vehicles such as pedelecs, is opening up new approaches for delivery over the so-called last mile. In this context, [1] points out the superiority of electrified cargo bikes over conventional vehicles in terms of life cycle assessment. Cargo trailers can be seen as an addition to cargo bicycles and are used to transport heavy and larger goods. Compared to conventional bicycle trailers, these are equipped with an electric drive to provide the increased power needed to carry heavy loads. However, considering the weight distribution of a system consisting of bicycle, rider and loaded trailer results in high demands on the control of the electric powertrain if it should also meet safety requirements. Thus, according to [2], the average weight of a man aged between 18 and 29 years in Germany is 79.6 kg. Combined with an average pedelec weight of 20 kg, this results in a total mass of the towing vehicle of approximately 100 kg. While the total weight of a trailer can be up to 250 kg according to [3]. In the fully loaded case, the towing vehicle must accelerate and decelerate 2.5 times its own mass. For this reason, the present work investigates the development of a control system that, in addition to convenient operation, contributes primarily to safety. Previous studies after [4, 5] deal mainly with system consisting of car and trailer, which intervene on the brakes of the vehicles or use active trailer steering to control the lateral dynamics. [6] proposes a control approach of trailers by controlling the car's yaw moment. While [7] gives a review on vehicle and trailer state and parameter estimation with a focus on the comparison of model based and non-model based estimation. Compared to the investigations described beforehand, the present research deals with a bicycle as the towing vehicle and a trailer that is self-propelled with an electric drive. Furthermore, the focus in the first step is on the design of a suitable controller for the longitudinal dynamics since the trailer presented here is not only to be towed by the bicycle but is to be self-propelled. The design and

testing of the vehicle dynamics longitudinal controller is performed on a real-time capable HIL system, which helps to avoid failures at an early stage of vehicle development.

Longitudinal Trailer Model

Based on a sketch of the system, which is limited to the longitudinal dynamics, the impact of the trailer forces on the towing vehicle can be visualized. In Figure 1 it can be seen that, in addition to the usual driving resistance forces, the force F_h acts on the towing vehicle when a trailer is attached.

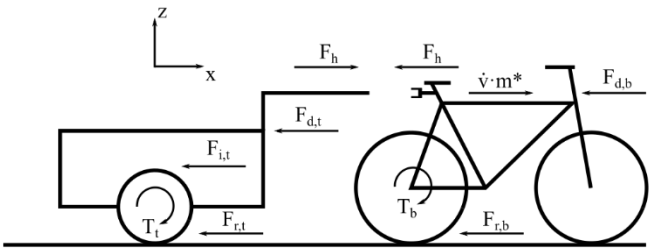

Figure 1. Forces acting on Bicycle and Trailer

Where F_d corresponds to the drag resistance, F_i to the inertial resistance and F_r to the rolling resistance of the respective system. While F_h represents the hitch force of the trailer that can apply pushing or pulling forces on the bicycle.

The torque T_b acting on the rear wheel of the bicycle results of the cyclist's pedal torque and the gears between the crank and sprocket cassette. Whereas the torque T_t only exists for self-propelled trailers that are equipped with a motor. The trailer considered in this investigation is equipped with a wheel hub motor for this purpose. The gradient resistance is neglected for both trailer and bicycle under the assumption of driving on an even road. Therefore, F_h is given in equation 1:

$$F_h = F_t - F_{r,t} - F_{i,t} - F_{d,t} \tag{1}$$

In which F_t results from the wheel torque T_t of the wheel hub motor divided by the dynamic rolling radius r_{dyn}. By formulating the individual driving resistances, equation 2 is obtained according to [8]:

$$F_h = \frac{T_t}{r_{dyn}} - m_t \cdot g \cdot c_r - \left(m_t + \frac{J_{red,t}}{r_{dyn}^2}\right) \cdot \dot{v} - \frac{\rho_{air} \cdot c_{d,t} \cdot A_t}{2} \cdot v^2 \tag{2}$$

The longitudinal dynamics of the towing vehicle are therefore given by equation 3:

$$\dot{v} \cdot m^* = F_b - F_{r,b} - F_{d,b} - F_h \tag{3}$$

Where m^* consists of the mass of the bicycle m_b and takes into account the moment of inertia $J_{red,b}$ of the rotating wheels:

$$m^* = m_b + \frac{J_{red,b}}{r_{dyn}^2} \tag{4}$$

This results in:

$$\dot{v} \cdot \left(m_b + \frac{J_{red,b}}{r_{dyn}^2}\right) = \frac{T_b}{r_{dyn}} - m_b \cdot g \cdot c_r - \frac{\rho_{air} \cdot c_{d,b} \cdot A_b}{2} \cdot v^2 - F_h \tag{5}$$

Where the acceleration $\dot{v}$ of the system can then be calculated via equation 6:

$$\dot{v} = \frac{\frac{T_b}{r_{dyn}} - m_b \cdot g \cdot c_r - \frac{\rho_{air} \cdot c_{d,b} \cdot A_b}{2} \cdot v^2 - F_h}{m_b + \frac{J_{red,b}}{r_{dyn}^2}} \tag{6}$$

The resulting speed v of the system, given by an integration of $\dot{v}$, is used to model the behavior of a driver that adjusts the torque on the pedals of the bicycle with a controller that tries to minimize the error between the present speed v and a speed reference v_{ref}. The maximum torque of an average cyclist as well as its cyclic output are modeled according to [9] using a sine wave with an amplitude of 25 Nm as well as an offset of 25 Nm and a frequency of approx. 1 Hz. By multiplication with a gain controlled by the driver PI-controller, the rider model can adjust the torque output. A simple gear ratio of $i_1 = 1.07$ and $i_2 = 0.93$ is assumed as a simplification for the purpose of this first study. These gear ratios are taken from the test bike, which is used for reference runs. The numbers are obtained using the smallest chainring in combination with the two highest numbers of teeth on the rear sprocket. The timing for a gear change to the lower ratio is selected when a speed of approx. 0.80 ms^{-1} is exceeded. Table 1 shows the parameters of the towing vehicle and trailer model that were used for the simulation:

Table 1. Parameters for simulation

System	Parameter	Unit	Value
General	g	ms^{-2}	9.81
	ρ_{air}	kgm^{-3}	1.20
	r_{dyn}	m	0.25
	c_r	-	0.027
Bicycle	m_b	kg	100
	$J_{red,b}$	kgm^2	0.11
	$c_{d,b}$	-	1.10
	A_b	m^2	0.54
Trailer	m_t	kg	115.10
	$J_{red,t}$	kgm^2	0.21
	$c_{d,t}$	-	1.20
	A_t	m^2	1.10

General assumptions include that the acceleration due to gravity is considered with 9.81 ms^{-2}. Furthermore, the air density ρ_{air} results at sea level and a temperature of 20°C in 1.20 kgm^{-3} according to [10]. In the context of this research, the dynamic tire radius r_{dyn} is approximated by half the diameter of a 20 inch wheel. According to [11], the rolling resistance coefficient c_r results in approximately 0.027 for a special tire for bicycle cargo applications. For the purposes of this study, it is assumed that both the bicycle and the trailer have the same 20 inch tire. As mentioned before, the mass of the towing vehicle m_b results from a bicycle mass of 20 kg and a driver mass of 80 kg. The wheels are taken into account with a mass of approximately 4.50 kg. The moment of inertia of rotating parts on the bicycle is limited to the front and rear wheels. Since these, in contrast to the trailer, do not have a hub motor, it results in an inertia of 0.11 kgm^2. The position of the driver's seat on the towing vehicle is assumed to be upright, which results in a drag coefficient $c_{d,b}$ of 1.10 and a frontal surface area of bicycle and rider A_b of 0.54 m^2 following the analysis of [12]. The mass of the trailer m_t is composed of an unloaded net weight of 49.10 kg and a load of 66 kg, resulting in a total weight of 115.10 kg regarding the presented simulation. Since the load on trailers can change quickly, which has a major impact on the driving resistance of the system, methods according to [13–16] can be used to estimate the load during operation. The rotating wheels account for 12.20 kg of the mass. Because the wheel hub motors weight of approximately 6 kg, the rotational moment of inertia $J_{red,t}$ of the trailer, results in 0.21 kgm^2. Since the trailer's front wall is perpendicular to the ground, the drag coefficient of the trailer $c_{d,t}$ is assumed to be completely upright according to [12], resulting in a value higher than the cyclist. Therefore $c_{d,t}$ is taken into account with a value of 1.20. Whereby the measured frontal surface area A_t is approximately 1.10 m^2. The vehicle dynamics model is completely implemented in SIMULINK.

Evaluation Strategy

In order to evaluate a developed longitudinal dynamics controller, several steps are needed, which are shown in Figure 2.

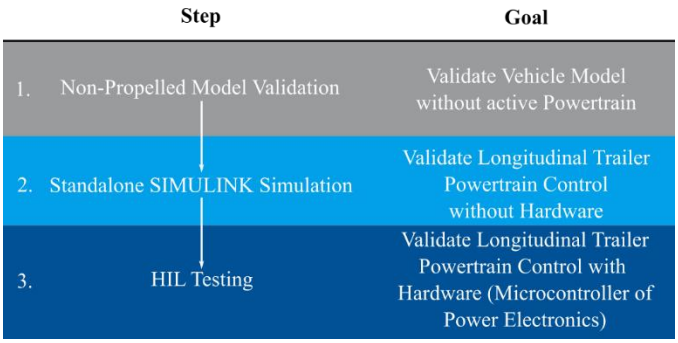

Figure 2. Evaluation Strategy Scheme

First, the developed model is compared with a real test drive, where both the model and the prototype of the test drive are not propelled by the hub motor. Therefore, the model's ability of following the measured velocity trajectory $v_{ref,1}$ of the real test drive is analyzed. In comparison with the measured data, it can be determined whether the model is parameterized sufficiently accurate, so the simulation reflects a representation of reality. Subsequently, in a second test case, it is investigated whether the model can follow a modified speed trajectory with higher required acceleration and maximum velocity $v_{ref,2}$ which is based on the measured trajectory. If the model cannot follow this trajectory, this case provides the approach for testing the longitudinal dynamics control of the powertrain. Hence, in the ideal case, if the longitudinal dynamics controller is adjusted appropriately, the required force F_h to pull the trailer is reduced by the engine and the driver can follow the second velocity trajectory with an actively driven trailer as well. The controller required for this is designed in SIMULINK and tested in the first step with a standalone SIMULINK vehicle dynamics simulation. If this step is successfully completed, the controller and the vehicle dynamics model can additionally be tested in interaction with parts of the hardware of the real powertrain in the context of a HIL setup. In this context, it is evaluated whether the designed vehicle dynamics control still provides a target-oriented result in combination with the control algorithms of the power electronics. For the SIMULINK standalone simulation as well as for the HIL testing, the curves of speed v, hitch force F_h and the required torque of the cyclist at the crank T_p are compared. Regarding the speed, the focus is on the possibility of the model to follow the given reference speed. In terms of F_h, it is investigated whether force peaks and the average can be reduced and whether a reduction in the pushing force can be achieved while braking the trailer. Concerning the required T_p, it is further investigated whether a reduction of peaks as well as of the average takes place.

Non-Propelled Model Validation

To ensure that the model follows the physical conditions, and that the rider's controller can follow a reference trajectory, the first step is to investigate a bicycle-trailer model without an active powertrain of the trailer (PT-off). The reference trajectory of $v_{ref,1}$ is obtained from a test drive of a trailer, which corresponds to the parameters listed in Table 1, where the system speed was measured, and low pass filtered to achieve a smooth reference trajectory. $v_{ref,1}$. The test drive was carried out on an even ground, which leads to no elevation. The gradient angle in the simulation is therefore neglected and set to 0° in the context of the longitudinal dynamics. The velocity v is computed using the PT-off model which is based on equation 6 in combination with equation 2 where T_t is considered as 0 Nm because the hub motor is not propelled. $v_{ref,1}$ and v as well as the required torque T_p at the crank to achieve the desired speed state are shown in Figure 3.

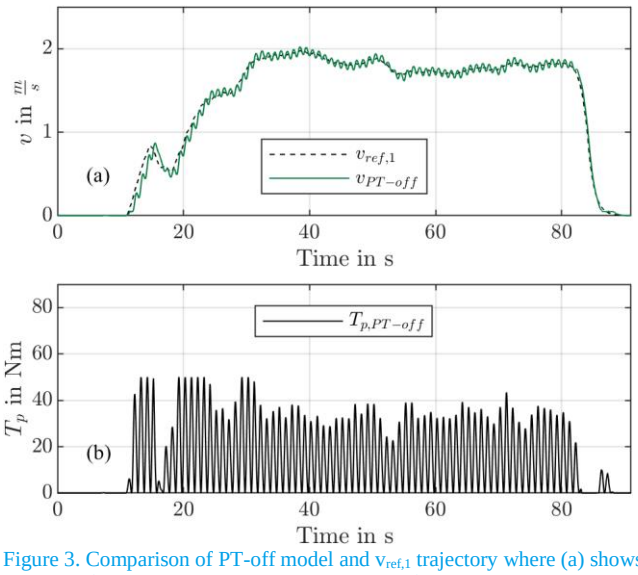

Figure 3. Comparison of PT-off model and $v_{ref,1}$ trajectory where (a) shows the velocity of the model and (b) shows the graph of T_p

The PT-off model's error values from the reference trajectory are shown in Table 2. As can be seen in Figure 3 (a), the model manages to follow the behavior of the reference trajectory of $v_{ref,1}$. This behavior is also reflected in the low values of the mean square error (MSE), sum square error (SSE) and root mean square error (RMSE). It is further noticeable that the cyclic torque output of the cyclist model is visible as a sinusoidal harmonic on the velocity signal. As in real conditions, the cyclist stops pedaling when braking, which is why the sinusoidal wave overlapping ends at about 82 s during deceleration. By looking at Figure 3 (b) it can be seen that the maximum available of 50 Nm provided by the cyclist is only required at the beginning. In the constant speed range from 40 to 80 s the required torque to follow the curve of $v_{ref,1}$ drops to values lower than 40 Nm. Therefore, it becomes clear that the cyclist can follow the curve of $v_{ref,1}$ with the available maximum torque. The speed signal v_{meas} of the raw data measured with the prototype from which $v_{ref,1}$ is generated by filtering is shown in Figure 4. In order to make a comparison between the real measurement run and the simulation, v_{meas} and the simulated speed v_{PT-off} resulting from $v_{ref,1}$ are listed in Figure 4. When comparing the data, it becomes evident that they exhibit a good qualitative agreement in case of acceleration, steady state and deceleration phase. Compared to v_{PT-off}, it is evident that v_{meas} has a sharper curvature of the oscillation superimposed on the fundamental signal. The larger and not exactly sinusoidal shaped superposition of v_{meas} results from the humans not optimally sinusoidal pedaling anatomy, which is not covered in the simulation. Further, the signal from v_{PT-off} is consistently below the signal of v_{meas}. The filtering of v_{meas} leads to a reduction of the amplitude, so that $v_{ref,1}$ is already lower than v_{meas} causing the simulated driver to stop the acceleration at slightly lower speeds.

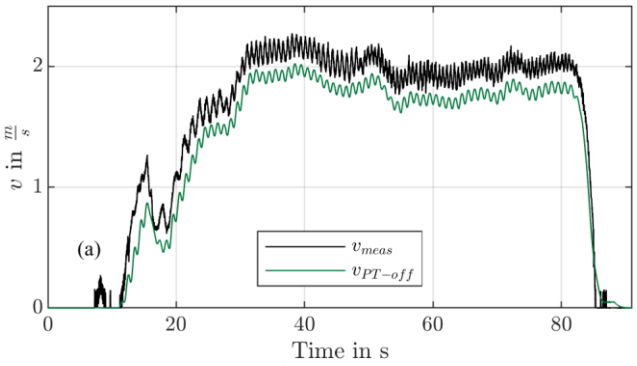

Figure 4. Velocity comparison of measured speed and simulated speed with PT-off model

With a second validation, it is examined whether the PT-off model can follow the $v_{ref,1}$ signal multiplied by a gain factor of 2 which is defined as $v_{ref,2}$. In comparison to the first case, the multiplication operation leads to an increase of the required acceleration to follow the $v_{ref,2}$ signal and higher maximum velocity. The resulting velocity of the PT-off model and $v_{ref,2}$ are shown in Figure 5 for this case.

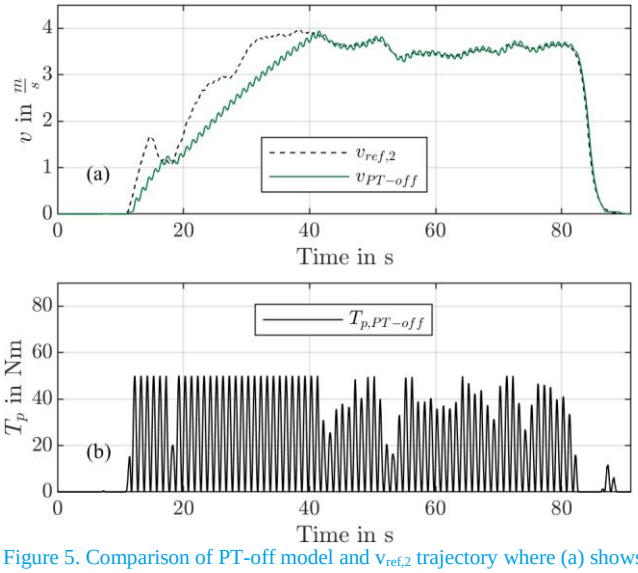

Figure 5. Comparison of PT-off model and $v_{ref,2}$ trajectory where (a) shows the velocity of the model and (b) shows the graph of T_p

As can be seen in Figure 5 (a), the driver does not manage to follow the $v_{ref,2}$ trajectory in the range between 12 and 40 s. According to Figure 5 (b) the limiting factor is the maximum torque T_p at the crank, which is not sufficient to apply the required acceleration. As can be seen from 12 to 40 s during acceleration phase the cyclist provides his maximum torque but isn't able to follow $v_{ref,2}$ because the driving resistances overcome the propulsion force. This behavior is confirmed by comparing the error values with the previous trajectory, which can be seen in Table 2. With MSE, SSE and RMSE values of 0.13, 912.42 and 0.35, the PT-off model has a significantly higher deviation in the second case than in the first case examined.

Table 2. Error values of v PT-off model in comparison to v_{ref}

Case	MSE	SSE	RMSE
$v_{ref,1}$	0.01	23.01	0.06
$v_{ref,2}$	0.13	912.42	0.35

Since the model can follow the $v_{ref,1}$ trajectory that was measured under real world conditions, the controller's driving behavior is considered to be close to reality. At this point, it is noted that each human input is different. Thus, the modeled controller behavior cannot represent all human characteristics.

Powertrain Simulation

The powertrain simulation is entirely done on a Typhoon HIL 604 in the Typhoon HIL modeling environment. The HIL System can be structured into two levels, that include real hardware and simulations running directly on the HIL.

The central part of the HIL system is a Typhoon HIL 604 on which the battery, inverter and motor are simulated. Since the present work is an investigation of vehicle dynamics, the battery is modeled in a generic way. The model used has a nominal voltage of 48 V and a capacity of 21 Ah. At the start of the simulation, the battery's state of charge is 80%, so the possibility of recuperation already exists from the beginning. The inverter is modeled as a simple B6 bridge, which

is controlled by real signals. These input pulse-width modulation (PWM) signals for the switching elements of the inverter are provided by an external hardware which uses a STM32F405 processor that is directly connected to the digital and analog connectors of the HIL. The motor control of the processor corresponds to the current open source project VESC according to [17] and uses field oriented control (FOC) as well as PWM generation based on space vector modulation. To compute the FOC algorithm, various analog and digital signals, which are normally measured on the inverter, must be made available to the processor as outputs from the HIL. These measurements are performed in the simulation and have to take care of the complete hardware signal processing chain from the sensor to the input of the controller. For example, the modeling of a current measurement via shunt contains a model of the shunt, measurement amplifier with offset and gain and a hardware filter if present in the real system. The following analog signals are provided from the HIL:

- DC voltage U_{DC}
- AC voltage U_{AC}
- AC current for each phase I_{AC}
- Motor and Mosfet temperature T_{Mot} and T_{Fet}

The modeling of the electrical system of the power electronics is based on the open source circuit diagram of the VESC 6 MK5 hardware according to [18]. Furthermore, the HIL System has to simulate the Hall sensor motor position measurements and provide them to the STM32F405. If provided accurately, the PI-Controller of the STM32f405 tries to follow the $i_{q,ref}$ current which can be given as an external CANBUS signal. Integrating the real processor of the power electronics ensures that the controller behavior of the drive train is mapped realistically. In addition to the FOC, the power electronics used has various estimation methods for position determination and restrictions, such as a limitation of the maximum DC current, which can be taken into account as well. In this way, it can be evaluated whether the FOC motor control and the higher-level vehicle dynamics control to be developed interact with each other as intended. Otherwise, this cascaded control structure that is shown in Figure 6 can lead to unwanted behavior such as instabilities.

The complexity of controlling a bicycle-trailer system as visualized in Figure 6 in a target-oriented way is explained by the components of the hitch force F_h listed in equation 2. Since F_h only exists during trailer operation and this force is mainly responsible for the comfort and safety of the towing vehicle, the aim of the present controller design is to minimize F_h with the target of 0 N. Assuming that there is no propulsion by the trailer. F_h results from the driving resistances of the longitudinal dynamics. Since these depend on the periodic torque of the cyclist, they occur with a superimposed sine wave. If an additional propulsive force of the system is now introduced via the powertrain of the trailer, this must theoretically be the same as the driving resistances which counteract the forward movement to ensure F_h can be reduced to 0 N. If the propulsive force resulting from T_t is too small, there is still a pulling force F_h which the driver must overcome. If the propulsive force is higher than the driving resistances in the current state of the bicycle trailer system, the resulting force F_h becomes positive and leads to a pushing behavior of the trailer.

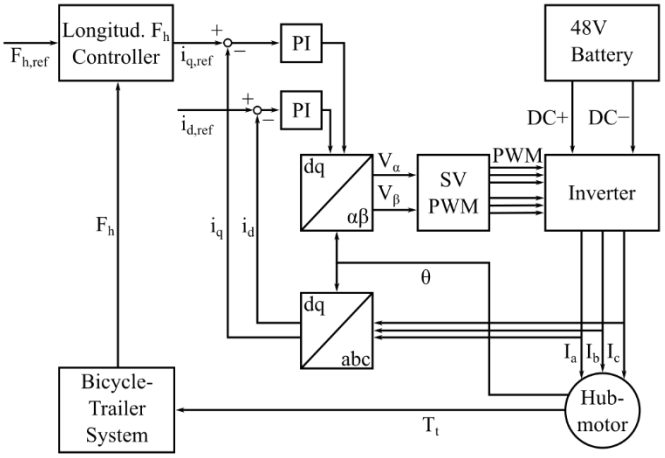

Figure 6. Cascaded Control Structure of FOC Motor Control and Longitudinal F_h Controller

The motor is modeled as a three-phase permanent magnet synchronous machine with a full-pole rotor. The motor parameters determined for the MXUS XF39 motor used are listed in Table 3. Determination is carried out with the internal estimation algorithms of the power electronics, since no data sheet from the manufacturer is available. The engine parameters were determined at a nominal temperature of 20°C.

Table 3. Motor parameters used in the simulation

Parameter	Value	Unit
p	23	-
R_s	0.0905	Ω
ψ_{PM}	0.022	Wb
L	80,29	µH
J_{mot}	0.0835	kgm²

The resulting torque T_t of the motor is given by the equation 7 according to [19]:

$$T_t = \frac{3}{2} \cdot p \cdot (\psi_d \cdot i_q - \psi_q \cdot i_d) \tag{7}$$

For the field control range the condition i_d = 0 A is valid. Therefore, equation 7 for T_t can be simplified as:

$$T_t = \frac{3}{2} \cdot p \cdot \psi_d \cdot i_q \tag{8}$$

After measurement and estimation of the motor parameters by algorithms of the power electronics, calculation of the PI current controllers is carried out. According to [17] the parameters K_p and K_i of the current controllers result in a value of 0.0803 for K_p and a value of 90.50 for K_i.

The simulation is completed by an integration of the previously described vehicle dynamics model consisting of the bicycle, driver and trailer, which is integrated into the powertrain simulation as a FMU. Figure 7 gives an overview of the complete HIL system.

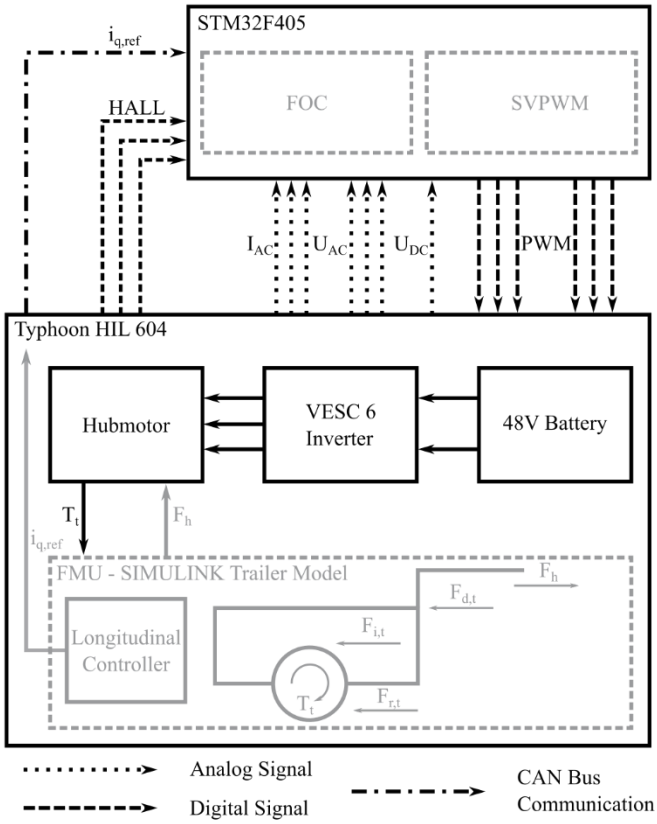

Figure 7. HIL System Overview

Longitudinal Model Predictive Controller

Regarding the shape of the F_h curve it is assumed that the periodic torque output of a cyclist which is described by [9] will lead to a sinusoidal superposition of the force curve of F_h, which should be kept at 0 N by the longitudinal dynamics controller. In this context, it must be considered that the torque output of the trailer drive can amplify the peaks due to non-optimal control, which can lead to an amplification of the already existing force peaks. This behavior is shown as an example in Figure 8 by the superposition of the hitch force $F_{h,raw}$ with the propulsive motor force $F_{t,1}$ resulting in $F_{res,1}$. Thus, while the negative force peaks are not reduced, points of $F_{h,raw}$ previously at 0 N are converted to positive values, increasing the peak-to-peak values of $F_{res,1}$. The expected driving behavior is classified as uncomfortable.

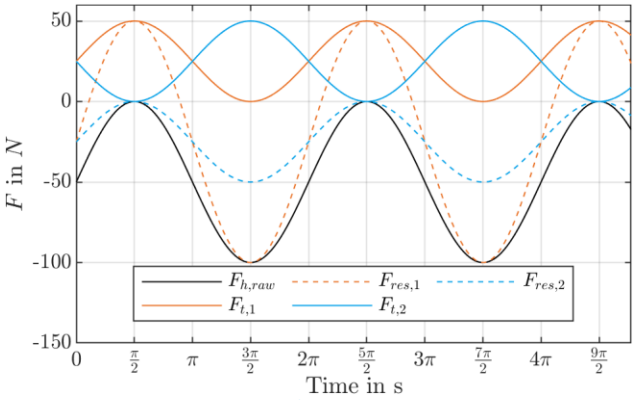

Figure 8. Exemplary illustration of the ideal sinusoidal superposition

By an optimized superimposition of the $F_{h,raw}$ curve with the propulsive motor force $F_{t,2}$ by a 180° phase shift, the peak forces can be damped, and the average force values can be reduced. Since the required motor torque T_t is adjusted by the power electronics which has its own control system, there is a time delay until the desired torque is applied. This delay, caused by the inertia of the system and the PI controllers of the FOC, must be considered by the longitudinal dynamics controller. As a result of these points, a predictive planning control is therefore useful to ensure an optimized $i_{q,ref}$ decision to keep F_h at 0 N. The existing setup will be used to evaluate whether the longitudinal F_h controller can be designed using MPC. The controller development is carried out in SIMULINK to be able to access the resources and toolboxes of SIMULINK during the design of the controller. However, since the integration of the vehicle dynamics model and the controller into the overall model is done via an FMU, source code must be generated from the SIMULINK model. Thus, after code generation, changes to the model or controller can only be made to the source code. To avoid this step, the SIMULINK model is extended with a substitute model of power electronics and motor. Thus, the controller can be completely designed in SIMULINK. Subsequently, the vehicle dynamics model and the designed controller can be integrated as FMU into the powertrain simulation on the HIL system, so that the controller can be tested with a more detailed model of the powertrain.

To characterize the combination of the power electronics processor using FOC and a simulated motor, a transfer function is formed using the HIL system. A powertrain model without vehicle dynamics components and only with the inertia of the engine is used in this context. Afterwards the input of the controller on the STM32F405 is provided with a jump of the $i_{q,ref}$ signal from 0 to 10 A which is transferred via CANBUS. The resulting torque is converted to the tire force F_t and determined at v = 0 ms^{-1}. Therefore, it is only valid for the field control range. F_t is then used to calculate the force of the motor acting on the trailer against the driving resistances. Figure 9 shows the time domain data of the $i_{q,ref}$ signal and the measured force $F_{t,meas}$, which is slightly delayed with a constant value $F_{t,avg}$ of about 25 N.

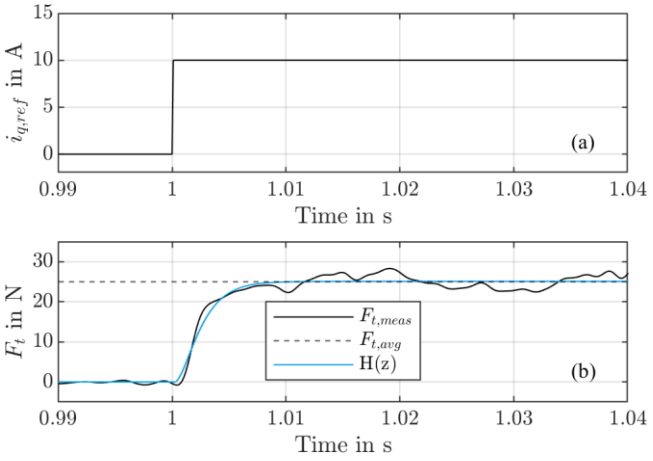

Figure 9. Step response of powertrain, where (a) shows the $i_{q,ref}$ input and (b) visualizes the corresponding measured and transfer function output

The transfer function can be approximated with the discrete transfer function $H(z)$ which is given in equation 9. The estimation was carried out with the system identification toolbox in MATLAB:

$$H(z) = \frac{0.0143}{z^2 - 1.8474 \cdot z + 0.8531} \tag{9}$$

With the help of the transfer function, the MPC controller can be designed, where the input of the transfer function $i_{q,ref}$ forms the manipulated variable m_v of the controller, while the output of the transfer function F_t acts on the driving dynamics of the trailer. A positive value of $i_{q,ref}$ ensures that the controller uses the drive to support the bicycle when it accelerates. At the same time, the additional force applied by the trailer is reduced when the bicycle decelerates due to regenerative operation of the powertrain caused by a negative $i_{q,ref}$ value. Finally, F_h which is the measured output m_o of the system can be acquired and returned to the controller.

The objective of the longitudinal dynamics controller is to adjust the amount of engine torque in a way that the hitch force F_h in the drawbar is reduced to 0 N. As a result, the driver of the tractor-trailer combination does not notice the trailer. This applies both to acceleration, driving at constant speed and braking. For safety aspects, braking is an important part of the process, because otherwise the trailer may push the bicycle and the rider. This can lead to an increase in braking distance or jackknifing. The purpose of this research is to evaluate whether these objectives can be satisfied for the presented system with a controller using MPC. As a result, the MPC should be used to minimize the error e_{FH} between the reference hitch force $F_{h,ref}$ and the measured hitch force F_h:

$$e_{FH} = \min\left(F_{h,ref} - F_h\right) \tag{10}$$

Where $F_{h,ref}$ corresponds to 0 N to ensure the goal of no additional force in the hitch. The measurement of F_h in the model is based on equation 2 with a one timestep delayed value of $\dot{v}$ while in reality it can be implemented using a drawbar with load cells according to [20]. To enable comfortable operation, the controller must be able to compensate for the sinusoidal oscillations of the F_h signal by implementing the phase shift principle described in Figure 8. Based on a cadence of about 1 Hz in which the driver applies the torque to the system, the maximum of the sine wave occurs after 0.25 s. In this period, the controller should react. For this reason, the time step T_s of the controller is determined with approx. 20% of 0.25 s to 0.05 s. The prediction horizon p is currently chosen with 20 time steps and the control horizon m_c at 2 time steps to keep the computational effort low. The controller is designed to support acceleration with positive motor torque and to support braking with negative motor torque. For this reason, the MPC control range is limited to $i_{q,ref}$ values between 0 and 70 A in the basic state, which corresponds to acceleration and steady state driving. The threshold value of $\dot{v}$ for detecting braking is currently set to -0.80 ms^{-2} and results from tests carried out with the trailer prototype. At values of $\dot{v}$ smaller than -0.80 ms^{-2} the $i_{q,ref}$ range is limited to values between 0 and -70 A. In this way, it can be ensured that a briefly reduced acceleration due to the cyclic torque of the cyclist does not cause braking during a longer acceleration or constant speed. In this way, braking is only supported when it is truly detected, so that comfort and safety can be brought in line with each other.

MPC Controller Testing

At the beginning of the development, the designed controller is tested without the HIL system in a standalone SIMULINK simulation. It will be investigated if it is possible to achieve a reduction of F_h and the pedal torque of the driver T_p while the driver follows the profile of $v_{ref,1}$ and $v_{ref,2}$. Finally, the MPC longitudinal dynamics controller will be integrated into a more detailed powertrain simulation in the Typhoon HIL environment so that its interaction with the microcontroller of the power electronics can be tested.

Standalone SIMULINK Simulation

The first step is to investigate the effects of the model with MPC powertrain control (PT-MPC) turned on in comparison to the PT-off model when following the $v_{ref,1}$ trajectory. For this case, the signals of v, F_h and T_p for both models are shown in Figure 10. As can be seen in Figure 10 (a), the driver can accelerate the vehicle to the desired speed even without the active drive train of the trailer. However, an increased amount of tractive force is required for this, as can be seen in Figure 10 (b). Sinusoidal oscillations, some of which exceed peak-to-peak values larger than an absolute value of 100 N, force the driver to apply increased torque to the crank if the trailer drivetrain is not used. In the range between 11 and 82 s, the average force is -34.90 N. During deceleration, the force reaches a peak value of 62.12 N, which additionally pushes the bicycle forward. The average torque of the cyclist is 17.33 Nm with peaks above 30 Nm required almost consistently to follow $v_{ref,1}$ as can be seen in Figure 10 (c).

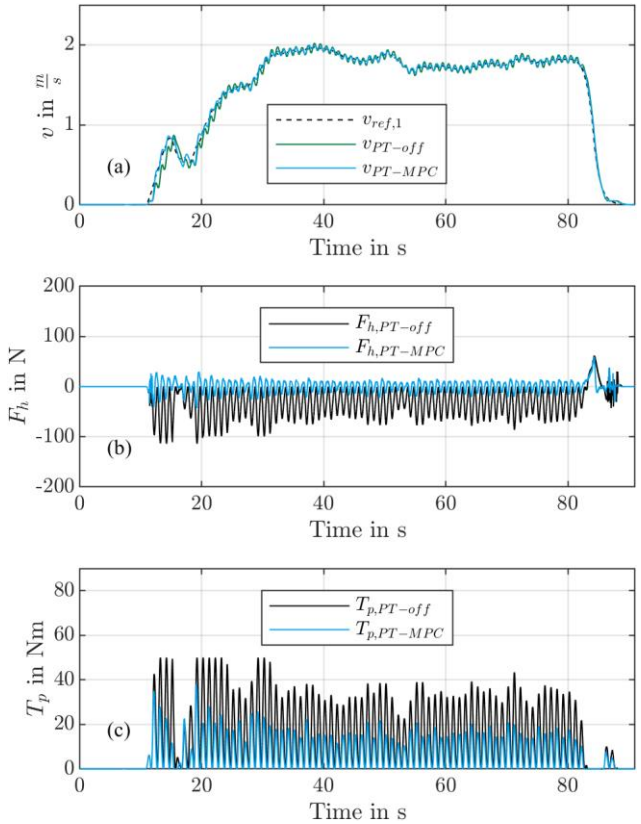

Figure 10. Comparison of PT-off and PT-MPC model while following the $v_{ref,1}$ trajectory where (a) shows the velocity of the models, (b) shows the graph of F_h and (c) shows the graph of T_p

If the MPC controller of the drive train is activated, it can be seen in Figure 10 (a) that the curve of $v_{ref,1}$ can be tracked even better. This is reflected in Table 4 as well. With values of MSE, SSE and RMSE of 0.01, 8.04 and 0.03, this model has a lower error in comparison to the PT-off values of Table 2. Furthermore, it can be seen in Figure 10 (b) that the active drive train can reduce F_h with an average of 0.32 N. The peak-to-peak values of the amplitudes can be reduced to an absolute value of approximately 60 N during acceleration and around 30 N while steady-state driving, between approx. 40 and 80 s. During deceleration, the force of the trailer can be reduced slightly with a value of 59.80 N, compared to the PT-off simulation. Furthermore, it can be seen in Figure 10 (c) that the required torque at the crank also drops to an average of 7.94 Nm, whereby the values are almost always below 20 Nm during steady-state driving.

Finally, in the second comparison, v, F_h and T_p are compared for the PT-off and the PT-MPC model when following the $v_{ref,2}$ trajectory. The signals of the two models are shown in Figure 11. As can be seen in Figure 11 (a), the driver does not manage to follow $v_{ref,2}$ in the PT-off simulation. Only after approx. 40 s the driver reaches the desired final speed and can maintain it. In Figure 11 (b) F_h with an average of -42.99 N and several peaks up to an absolute value of 100 N and partly larger is evident. When decelerating the vehicle from a higher speed in the same time period, a force of 150.12 N results. The driver must additionally handle this force. As can be seen in Figure 11 (c), the driver needs his full torque of 50 Nm at the crank when accelerating over a longer period of time. In the course of time, the torque required by the driver in the PT-off model decreases slightly, but remains partly above 40 Nm in the stationary range between 40 and 80 s.

With MPC powertrain control turned on, the driver in the PT-MPC model can follow the trajectory of $v_{ref,2}$ as desired in Figure 11 (a). Regarding Table 4 this is reflected by MSE, SSE and RMSE values of 0.01, 22.18 and 0.06 with a lower error compared to the PT-off model for this case. The force F_h in Figure 11 (b) decreases to 0.11 N on average and shows absolute peak-to-peak values of approximately 30 N in the area with stationary speed. In the PT-MPC model, F_h is reduced to only 57.71 N during deceleration. The reduction of F_h of nearly three times compared with the PT-off model during deceleration contributes to the safety of the system since the driver has less additional force that pushes him. It is evident in Figure 11 (c) that the driver needs considerably less torque at the crank, with an average of 9.73 Nm to drive the system. In the stationary speed range, the driver needs a torque below 20 Nm for most of the time.

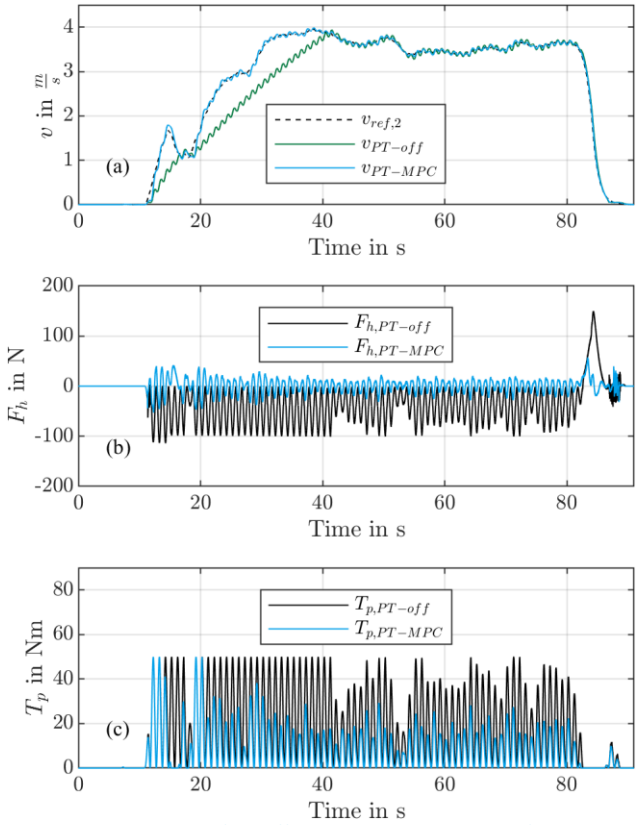

Figure 11. Comparison of PT-off and PT-MPC model while following the $v_{ref,2}$ trajectory where (a) shows the velocity of the models, (b) shows the graph of F_h and (c) shows the graph of T_p

Table 4. Error values of v PT-MPC model in comparison to v_{ref}

Case	MSE	SSE	RMSE
$v_{ref,1}$	0.01	8.04	0.03
$v_{ref,2}$	0.01	22.18	0.06

HIL Testing

After the SIMULINK standalone simulation has shown that a reduction of F_h as well as T_p is possible with the help of the MPC powertrain control, the developed controller is tested on the HIL system. The aim is to determine whether target-oriented control can

be achieved using the STM32 hardware and a detailed motor model. In contrast to the SIMULINK standalone simulation, the vehicle dynamics control and the vehicle dynamics model are integrated as FMU into the Typhoon HIL powertrain simulation. The MPC controller within the FMU calculates the $i_{q,ref}$ and does not send it to the motor and power electronics transfer model, but directly to the STM32F405 via CANBUS. The STM32F405 controller calculates the required PWM signals and passes them to the HIL via digital input pins. The B6 circuit simulated in the HIL then generates an AC current, which is transferred to the motor model. The resulting torque of the machine in turn serves as input for the vehicle dynamics simulation of the FMU. For testing the longitudinal dynamics controller, it is examined whether the driver manages to follow the $v_{ref,1}$ and $v_{ref,2}$ trajectory with the help of the active MPC controller in combination with a detailed powertrain simulation.

The first test on the HIL system therefore shows the subsequent behavior of the trailer system with respect to $v_{ref,1}$. Figure 12 shows v, F_h and T_p of the models of PT-off as well as PT-MPC. The PT-MPC model is executed on the HIL, providing a realistic simulation of the motor and inverter behavior.

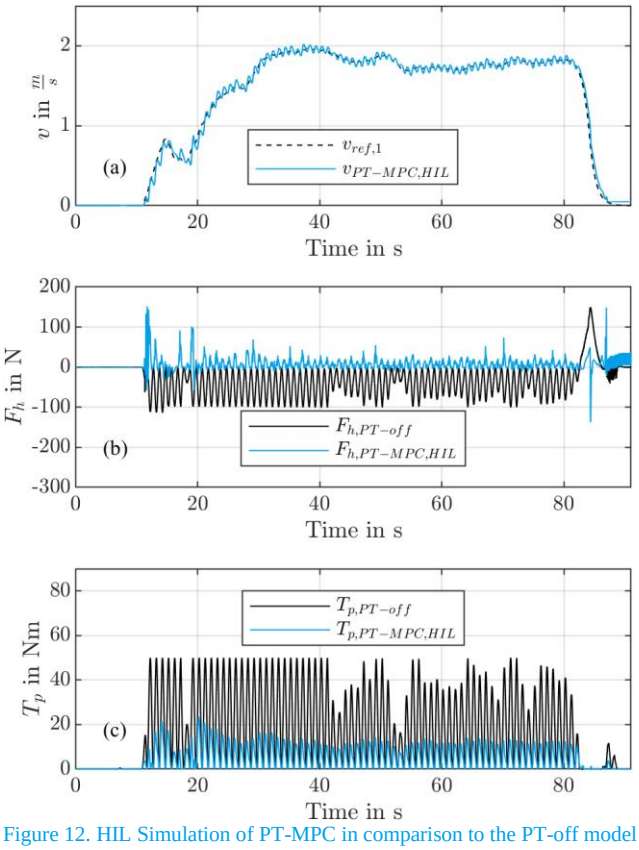

Figure 12. HIL Simulation of PT-MPC in comparison to the PT-off model while following the $v_{ref,1}$ trajectory where (a) shows the velocity of the models, (b) shows the graph of F_h and (c) shows the graph of T_p

As can be seen in Figure 12 (a), the cyclist can follow the trajectory of $v_{ref,1}$. This behavior is reflected in the error values MSE, SSE and RMSE of the PT-MPC,HIL model compared to the $v_{ref,1}$ trajectory with values of 0.01, 23.01 and 0.05 in Table 5, respectively. Compared to the PT-off model in Table 2, the PT,MPC,HIL model has only a slightly better RMSE value, but the advantages of the active drive train are noticeable by a subsequent consideration of F_h and T_p. It can be seen from Figure 12 (b) that there is a significant reduction of F_h in the constant speed region on the HIL simulation, resulting in average F_h value of 7 N. In the constant speed region between 40 and 80 s the peak-to-peak average value of F_h can be reduced to around 30 N. As the driver starts to accelerate F_h peaks up to 150 N are present. This positive F_h curvature at the beginning, causes the trailer to push the cyclist. It is similarly reflected in Figure 12 (c), where a significant reduction in the torque required at the rider's crank can be seen at the beginning for the PT-MPC model compared to the PT-off model. Where the average value of T_p can be reduced to 4.72 Nm with peak-to-peak vales in the constant speed range smaller than 15 Nm. During deceleration starting at 83 s, a rise of F_h can be recognized. At this point the MPC controller has not passed the $\dot{v}$ threshold value of -0.8 ms^{-2} and therefore no negative torque of the motor is applied. At 84 s the $\dot{v}$ threshold is passed and a negative $i_{q,ref}$ resulting in a negative motor torque on the trailer is applied. A F_h peak of -137.20 N pulls the system and supports the braking procedure. However, a short push of the trailer with an F_h value of 148 N follows briefly before standstill. This unsteady behavior results from the logic components, which assign limit values for the MPC control depending on the system state, as well as a small simulation delay caused by the FMU. As can be seen when tracking the trajectory of $v_{ref,1}$, oscillations of the system states are present, which lead to unsteady behavior as can be seen during braking. The HIL system makes it possible to detect these areas already in the development phase, so that an improvement in the simulation can be made in the first step, for example by readjusting the threshold values. With the help of HIL testing, this area can thus be classified as important in advance for test planning with the real trailer prototype.

The second test analyzes the behavior of the system with respect to $v_{ref,2}$. The resulting values of v, F_h and T_p are shown in Figure 13 in comparison to the PT-off model. Unlike the PT-off model, the PT-MPC,HIL model can follow the $v_{ref,2}$ trajectory in Figure 13 (a). Regarding Table 5 where the error of v against $v_{ref,2}$ is shown for the PT-MPC,HIL model, with 0.01, 72.46 and 0.09 this results in lower error values of MSE, SSE and RMSE compared with the PT-off model. Furthermore, considering Figure 13 (b), the PT-MPC,HIL model shows a reduction of the peak-to-peak values of F_h in the constant velocity range to about 35 N while the average value of F_h is at 7.54 N. During acceleration, an F_h peak of 127 N is obtained, which causes the trailer to push the cyclist slightly. During the deceleration, F_h first increases slightly up to a peak value of 46 N until the $\dot{v}$ threshold is exceeded. Then, with the help of the MPC control, a slightly pulling behavior of the trailer can be ensured, so that the cyclist is pulled with an absolute F_h value of 31.18 N. The slightly pushing behavior of the trailer during acceleration and constant speed operation is recognizable by looking at the T_p values in Figure 13 (c) as well. With an average T_p value of 6.06 Nm and peak-to-peak values smaller than 20 Nm when driving at constant speed, there is a significant reduction in the required driver torque compared to the PT-off model.

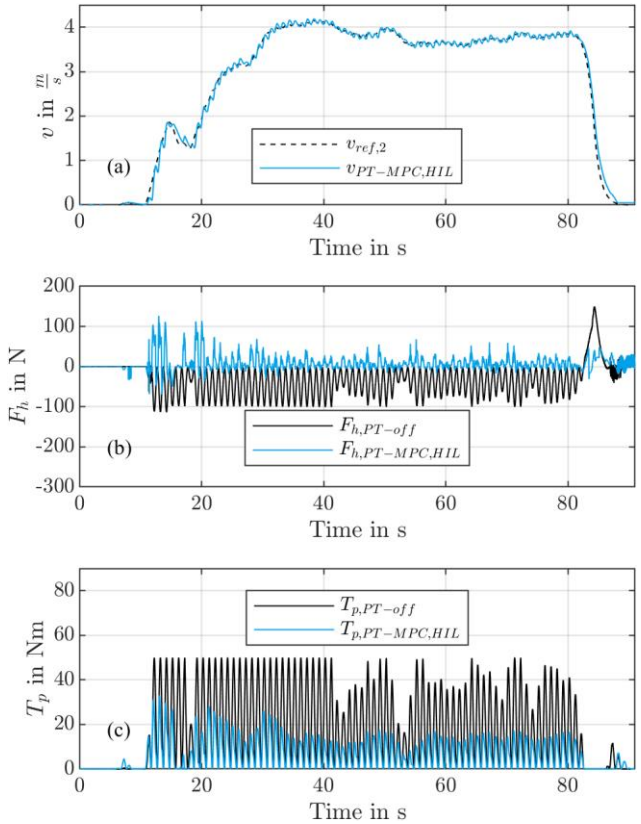

Figure 13. HIL Simulation of PT-MPC in comparison to the PT-off model while following the $v_{ref,2}$ trajectory where (a) shows the velocity of the models, (b) shows the graph of F_h and (c) shows the graph of T_p

Table 5. Error values of v for PT-MPC, HIL model in comparison to v_{ref}

Case	MSE	SSE	RMSE
$v_{ref,1}$	0.01	23.01	0.05
$v_{ref,2}$	0.01	72.46	0.09

Both simulations with active MPC controller indicate a reduction of the average required F_h and can achieve a damping of the F_h amplitude in the constant velocity range. To illustrate this, the time period 72 to 80 s from Figure 13 (b) is shown again in Figure 14. It is evident that for this range the absolute amplitude of F_h can be reduced from an average of 82.07 N for the PT-off model to an average of 32.11 N for the PT-MPC,HIL. As a result, the average amplitude of F_h can be reduced to about 40% of the amplitude from the PT-off model by the MPC longitudinal dynamics control.

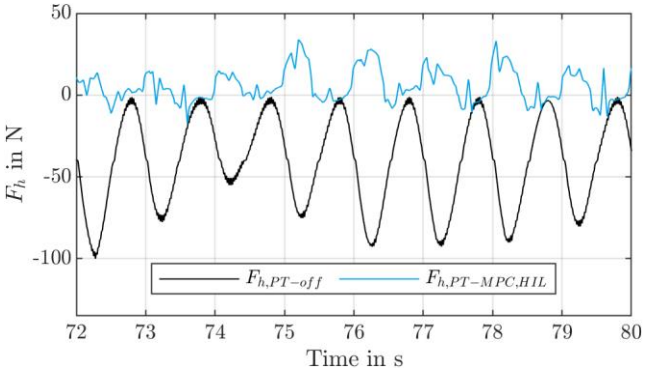

Figure 14. F_h for PT-off and PT-MPC,HIL model in the time period from 72 to 80 s while following the faster v_{ref} trajectory

The MPC longitudinal dynamics control presented enables damping of F_h, which, without active drivetrain control, exhibits a strong sinusoidal characteristic even in the constant speed range due to the periodically occurring torque of the cyclist. The force peaks that occur when the drivetrain is inactive lead to uncomfortable driving behavior of the system. By damping the amplitudes, this behavior can be reduced, resulting in a more comfortable ride. The average slightly positive values of F_h with active MPC powertrain control lead to smoother operation of the overall system and contribute to comfortable operation when driving with an electrified trailer. Despite the supportive operation by the active powertrain, the designed longitudinal dynamics controller manages to actively support the braking maneuvers presented and to prevent an additional thrust of the trailer. However, the positive F_h peak occurring at standstill when following the $v_{ref,1}$ trajectory must be avoided. In this context, it is advisable to limit the controller by logic operators at standstill. Furthermore, the presented MPC longitudinal dynamics controller is suitable for the implementation of different support levels of the trailer. These can be implemented by specifying $F_{h,ref}$. For example, positive $F_{h,ref}$ values can enable a pushing trailer that provides sufficient support for the driver. Negative $F_{h,ref}$ values lead to a pulling behavior of the trailer towards the bicycle, resulting in less comfort but safer operation.

Summary

In the presented research, the longitudinal dynamics control of an electrically driven cargo trailer for micromobility applications was investigated. In order to design the controller efficiently and to analyze the behavior of the controller interacting with a simulated driver and a lower level FOC motor controller, a HIL approach was chosen. The system consisting of an electrified trailer with complete drivetrain, bicycle and driver was modeled in SIMULINK and Typhoon HIL environment and is simulated in real time on a Typhoon HIL 604. By connecting the HIL system to the processor of the later used power electronics, the dynamical behavior of the electric machine and its controller are taken into account precisely. As a result of the periodic delivery of torque from a cyclist, there is a strong sinusoidal superposition of the hitch force curve when operating a regular cargo trailer. Depending on the mass being towed, the hitch force peaks can make operation uncomfortable. In addition, the inertia of the trailer during acceleration creates a large additional force that the cyclist must provide. In contrast, the driver must handle this additional force in the opposite direction during a braking maneuver as well.

For this reason, the present research investigated whether an MPC longitudinal dynamics controller can be used to fulfill the following requirements with the powertrain of an electrified cargo trailer:

- Provide assistive torque during acceleration.
- Increase comfort in the constant speed range by damping the hitch force amplitude.
- Enable safety-oriented trailer operation by reducing the hitch force during braking maneuvers.

By setting the reference hitch force to 0 N, the MPC controller attempts to set the $i_{q,ref}$ in a way that the resulting torque prevents an increase or decrease in the hitch force, which is measured in the drawbar between the trailer and the bicycle. An additional limitation of the control range depending on the system state, which can be limited to basic state and braking, made it possible to develop a control system that is generally target-oriented. Therefore, the MPC controller supports braking only if the acceleration falls below the value of -0.80 ms^{-2}. Existing outliers still need to be minimized in further development by transition areas of the control limitation. These constraints prevent random braking of the trailer at smaller negative accelerations, which can be triggered by the periodic torque output of the cyclist, for example. The presented MPC longitudinal dynamics controller can support the driver in a way that he can follow a slowly accelerated as well as a faster accelerated reference speed trajectory with higher final speed. In this case, a comparison model with the powertrain switched off does not manage to follow the faster reference speed trajectory without a long delay. In terms of reference speed trajectory tracking error, a trailer with the presented MPC longitudinal dynamics control manages to exhibit lower values of MSE, SSE and RMSE compared to a non-propelled trailer. At the same time, the use of the MPC longitudinal dynamics controller can reduce the torque required from the rider at the crank of the bicycle, in a way that comfort can be increased. This behavior is accompanied by a reduction of the hitch force amplitude compared to the inactive drivetrain, which can be achieved by the MPC. During braking, the trailer's drivetrain assists the system as soon as the acceleration threshold is passed, resulting in reduced positive hitch force values that would push the driver and instead converting them into negative, i.e., pulling hitch force values, which additionally decelerate the system. For the slow reference speed case, the pushing hitch force could be converted from a value of 62.12 N to a trailer pulling with -137.20 N. In the faster reference speed case, the pushing hitch force could be reduced from 150.12 N to 46 N at first and finally to a pulling force of -31.18 N. With these results, the MPC longitudinal dynamics controller contributes not only to an increase in comfort but also to an increase in safety during braking maneuvers.

Within the scope of the following investigations, more test cases must be analyzed to evaluate the functionality of the system. In this context, further test drives based on real cases in different characteristics such as different loading and different driver weight have to be investigated. These can include, for example, tests at extreme low or higher speeds and different acceleration and deceleration situations. In addition, a more detailed tire model as presented in [11] can be used to draw conclusions about the longitudinal slip conditions. Furthermore, it can be evaluated whether different support levels can be implemented in the controller by selecting the value of the reference hitch force. Depending on the choice of the reference hitch force, an electrified trailer with MPC longitudinal dynamics controller can be transformed into a pushing or pulling trailer. Based on the driver's preference, this corresponds to different support levels. At the same time, the constant setting of the reference hitch force can be replaced by a trajectory. With this implementation, a reference hitch force value of less or equal to 0 N can be set when a braking maneuver is detected. This ensures that the powertrain is supporting the deceleration with actively pulling the system until standstill. Additionally, the presented HIL system can be used for the constant controller development to investigate whether different loading states of the trailer require different controller parameterization. In this case, the controller can be supplemented according to [21], for example, by gain-scheduling depending on the load on the trailer.

Besides these improvements, it can be evaluated whether the use of nonlinear MPC contributes to an even stronger damping of the hitch force amplitudes, which makes the acceleration behavior smoother. While the present investigations have concentrated on the longitudinal dynamic area, the HIL setup offers the possibility of investigating the lateral dynamic behavior as well. By complementing the vehicle dynamics simulation with a lateral vehicle model, new approaches to suppress jackknifing and swaying with the powertrain and a higher-level lateral dynamics control can be investigated.

Conclusion

Within the scope of this work, a bicycle was simulated in combination with an electrically driven cargo trailer. It could be shown that the periodic torque of the driver affects the hitch force in the drawbar in case of sinusoidal superposition. This sinusoidal shape of the hitch force, which serves as an input parameter for the longitudinal dynamics control of the drive train, is problematic. If the hitch force is to be controlled to 0 N, the longitudinal dynamics controller must compensate for this effect. To achieve this, MPC was used and tested to control the powertrain based on the measured hitch force. In the course of HIL testing, it was additionally examined whether the MPC longitudinal dynamics controller interacts properly with the FOC of the power electronics. While a general positive interaction is given, the MPC's output-limiting logic still need to be optimized. Nonetheless, with the aid of the MPC controller, it was possible to attenuate the hitch force amplitudes and the required hitch force mean value during steady state driving. In addition, the MPC controller led to a reduction of the hitch force during braking. In conclusion, it can be said that with sufficient information about the system, which for example requires knowledge about the loading of the trailer, MPC longitudinal dynamics control can lead to an increase in comfort and an improvement in safety. Therefore, MPC longitudinal dynamics control has proven to be useful for controlling cargo trailers in micromobility to compensate for the periodic hitch force, making this approach suitable for further analysis.

References

1. Temporelli, A., Brambilla, P.C., Brivio, E., and Girardi, P., "Last Mile Logistics Life Cycle Assessment: A Comparative Analysis from Diesel Van to E-Cargo Bike," *Energies* 15(20):7817, 2022, doi:10.3390/en15207817.
2. Mensink, G.B.M., Schienkiewitz, A., Haftenberger, M., Lampert, T. et al., "Übergewicht und Adipositas in Deutschland: Ergebnisse der Studie zur Gesundheit Erwachsener in Deutschland (DEGS1)," *Bundesgesundheitsblatt, Gesundheitsforschung, Gesundheitsschutz* 56(5-6):786–794, 2013, doi:10.1007/s00103-012-1656-3.

3. CARLA CARGO Engineering GmbH, “eCARLA,” https://www.carlacargo.de/de/produkte/ecarla/, March 20, 2023.
4. Vempaty, S. and He, Y., “A Review of Car-Trailer Lateral Stability Control Approaches,” *SAE Technical Paper Series*, SAE Technical Paper Series, WCX™ 17: SAE World Congress Experience, APR. 04, 2017, SAE International400 Commonwealth Drive, Warrendale, PA, United States, 2017, doi:10.4271/2017-01-1580.
5. ZHAO, Z., ZHANG, N., WU, J., and YIN, G., “Model Predictive Control of Car-trailer combinations based on Differential Braking,” *2021 IEEE 5th Advanced Information Technology, Electronic and Automation Control Conference (IAEAC)*, 2021 IEEE 5th Advanced Information Technology, Electronic and Automation Control Conference (IAEAC), Chongqing, China, 12.03.2021 - 14.03.2021, IEEE, ISBN 978-1-7281-8028-1:2419–2424, 2021 - 2021, doi:10.1109/IAEAC50856.2021.9391063.
6. Zanchetta, M., Tavernini, D., Sorniotti, A., Gruber, P. et al., “Trailer control through vehicle yaw moment control: Theoretical analysis and experimental assessment,” *Mechatronics* 64:102282, 2019, doi:10.1016/j.mechatronics.2019.102282.
7. Korayem, A.H., Khajepour, A., and Fidan, B., “A Review on Vehicle-Trailer State and Parameter Estimation,” *IEEE Trans. Intell. Transport. Syst.*:1–18, 2021, doi:10.1109/TITS.2021.3074457.
8. Ersoy, M. and Gies, S., “Fahrwerkhandbuch,” Springer Fachmedien Wiesbaden, Wiesbaden, ISBN 978-3-658-15467-7, 2017.
9. Quintana-Duque, J.-C., Dahmen, T., and Saupe, D., “Estimation of Torque Variation from Pedal Motion in Cycling,” *International Journal of Computer Science in Sport*(Volume 14):34–50, 2015.
10. “VDI-Wärmeatlas,” Springer Berlin Heidelberg, Berlin, Heidelberg, ISBN 978-3-642-19980-6, 2013.
11. Miller, M., Pfeil, M., Reick, B., Murri, R. et al., “Measurement and Modeling of a Cargo Bicycle Tire for Vehicle Dynamics Simulation,” *Applied Sciences* 13(4):2542, 2023, doi:10.3390/app13042542.
12. Chowdhury, H. and Alam, F., “Bicycle aerodynamics: an experimental evaluation methodology,” *Sports Eng* 15(2):73–80, 2012, doi:10.1007/s12283-012-0090-y.
13. Altmannshofer, S. and Endisch, C., “Robust vehicle mass and driving resistance estimation,” *2016 American Control Conference (ACC)*, 2016 American Control Conference (ACC), Boston, MA, USA, 06.07.2016 - 08.07.2016, IEEE, ISBN 978-1-4673-8682-1:6869–6874, 2016 - 2016, doi:10.1109/ACC.2016.7526754.
14. Rhode, S. and Gauterin, F., “Online estimation of vehicle driving resistance parameters with recursive least squares and recursive total least squares,” *2013 IEEE Intelligent Vehicles Symposium (IV)*, 2013 IEEE Intelligent Vehicles Symposium (IV), Gold Coast City, Australia, 23.06.2013 - 26.06.2013, IEEE, ISBN 978-1-4673-2755-8:269–276, 2013 - 2013, doi:10.1109/IVS.2013.6629481.
15. Vahidi, A., Stefanopoulou, A., and Peng, H., “Recursive least squares with forgetting for online estimation of vehicle mass and road grade: theory and experiments,” *Vehicle System Dynamics* 43(1):31–55, 2005, doi:10.1080/00423110412331290446.
16. Miller, M., Pfeil, M., Reick, B., and Kennel, R., “Quasi-Static Approach for Mass Estimation of Electric Propelled Vehicles,” in: *PCIM Europe 2023*:991–1000, doi:10.30420/566091138.
17. Vedder, B., “GitHub - vedderb/bldc: The VESC motor control firmware,” https://github.com/vedderb/bldc/, March 24, 2023.
18. Vedder, B., “VESC 6 MK5,” https://vesc-project.com/sites/default/files/Benjamin%20Posts/VESC_6_mk5.pdf, April 21, 2023.
19. Typhoon HIL, “Three Phase Permanent Magnet Synchronous Machine: Description of the Three Phase Permanent Magnet Electrical sub-system model,” https://www.typhoon-hil.com/documentation/typhoon-hil-software-manual/References/three_phase_permanent_magnet_synchronous_machine.html, April 21, 2023.
20. Miller, M., Kaufmann, A., Reick, B., and Pfeil, M., “Intelligente Anhängerdeichsel für verschiedene Zugfahrzeuge,” Research Paper, Hochschule Ravensburg-Weingarten, Weingarten, 2021.
21. Adamy, J., “Nonlinear systems and controls,” Springer, Berlin, Germany, ISBN 978-3-662-65632-7, 2022.

Contact Information

Marius Miller: marius.miller@rwu.de

Definitions/Abbreviations

MSE	Mean square error
SSE	Sum square error
RMSE	Root mean square error
FOC	Field oriented control
PWM	Pulse-width modulation
MPC	Model predictive control
FMU	Functional mock-up unit

ISSN 0148-7191
https://saemobilus.sae.org/content/2023-24-0180